Modifications of detour phase computer-generated holograms

Uriel Levy, Emanuel Marom, and David Mendlovic

The detour phase method for the design of computer-generated holograms can be modified to achieve multichannel reconstruction along various diffraction orders. It is shown how a single hologram can be used to display two patterns of different intensities along two diffraction orders. This is achieved by the release of any requirement on the phase distributions of these patterns, thus leaving them as free parameters. Various algorithms are suggested to make possible nonidentical reconstructions along two different off-axis diffraction orders. The two reconstruction orders can be chosen arbitrarily. The case of four-channel reconstructions for generating four different images is discussed as well. Computer simulations and optical experiments were carried out to demonstrate the capabilities of the proposed approaches.

OCIS codes: 070.2590, 090.1760.

1. Introduction

Computer-generated holography was invented more than 30 years ago by Brown and Lohmann[1] and by Lohmann and Paris.[2] The idea relies on using a digital computer and a plotting device to imitate the interference pattern recorded by conventional holography. Computer-generated holography allows any arbitrary synthetic shape to be reconstructed, in contrast with conventional holography in which only a physical waveform can be recorded and then reconstructed.

The proposed encoding methods are based on the detour phase principle. According to this principle, the amplitude information and the phase information are modulated on a carrier grating. For encoding the amplitude the local width of a grating line is changed, while the phase information is encoded by the shift of the fringe position with respect to the center, as suggested by Brown and Lohmann[1] and by Lohmann and Paris.[2] A different approach that was based on multiple samples per cell rather than on a localized shift inside the cell was suggested by Lee[3] and by Burkhardt.[4]

A feature common to all the above methods is that the reconstruction can be obtained in any desired off-axis diffraction order. Nevertheless, other orders are generated as well. When Fourier plane reconstruction is involved, the 180°-rotated complex conjugate of the reconstruction appearing in a certain diffraction order will appear in its symmetrical order as well.

One of the most widespread applications of computer-generated holograms is beam shaping. Shaped beams can be used for a variety of applications, such as display, material processing, scanning, optical interconnection, and medicine. For these applications only the wave intensity is important. Therefore the phase distribution can be used as a free parameter to reduce the noise, increase the diffraction efficiency, and eliminate the speckle problem.[5] Alternatively, phase freedom can be used to achieve two desired patterns of different intensity distributions at two different planes along the Z axis, as suggested by Dorsch *et al*.[6] For implementing their approach a ping-pong algorithm for propagation and backpropagation between two planes was carried out. The constraints were the desired intensity in the two planes, while the phase was used as a free parameter.

In this paper we present a new approach that permits one to obtain, in the same plane z, two patterns having different intensities along two different orders by use of a simple binary mask. We show that the desired intensity patterns can be obtained in any plane (Fourier or Fresnel) for nonsymmetrical diffraction orders but in only Fresnel planes for symmetrical orders. One important advantage of this

The authors are with the Faculty of Engineering, Tel-Aviv University, 69978 Tel-Aviv, Israel.

Received 17 December 1997; revised manuscript received 20 January 1998.

0003-6935/98/143044-09$15.00/0

approach is that the diffraction efficiency is doubled compared with the basic detour phase approaches, since two orders are used rather than one. Therefore, for an amplitude-only hologram, a greater than 20% diffraction efficiency can be obtained rather than 10%, whereas for a phase-only mask a greater than 80% diffraction efficiency is expected.

The development of the relevant equations leading to the conventional reconstruction of two complex-conjugate patterns is reviewed in Section 2. In Section 3 the basic approach for achieving entirely different reconstructions along two symmetrical diffraction orders is described. Section 4 presents a generalization of Section 3. It provides a description of the techniques for determining the fidelity of each reconstruction in those two orders (Subsection 4.A), a simplified approach for achieving two nonidentical reconstructions (Subsection 4.B), an algorithm for achieving nonidentical reconstructions along any two diffraction orders (Subsection 4.C), and a combination of the above approaches with a two-dimensional encoding approach[8] for achieving four different-intensity reconstructions in four different diffraction orders (Subsection 4.D). In Section 5 we discuss the choice of parameters for implementing the approach. Computer-simulation results are given in Section 6, whereas experimental results are demonstrated in Section 7. Conclusions are given in Section 8.

2. Background

The detour phase approach is based on dividing the binary mask into an array of cells. Within each cell an aperture is drawn. A feature common to all detour phase approaches is that the out-of-center lateral shift of the aperture area identified as $a(x, y)$ inside the cell is limited by

$$\left|\frac{x_{\max}}{\Delta x}\right| = \frac{1}{2}, \tag{1}$$

where Δx is the lateral size of the cell. Since the reconstruction occurs along diffracted-beam directions, the local phase delay caused by this lateral shift is given by

$$\phi = \frac{2\pi x M}{\Delta x}, \tag{2}$$

where M is the desired diffraction order. The information diffracted toward the symmetrical order $-M$ is the complex conjugate of the information that appears in the $+M$ order. The field distribution of the Mth diffraction order is given by

$$H(x, y) = \int_{-\infty}^{\infty}\int_{-\infty}^{\infty} a(x', y')\exp[i\phi(x', y')] \times \exp[-i(2\pi x x' + 2\pi y y')]\mathrm{d}x\mathrm{d}y, \tag{3}$$

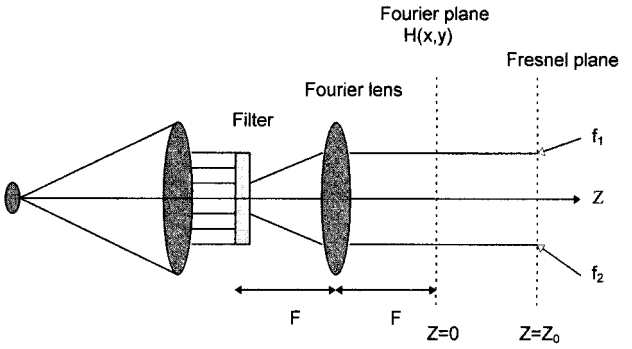

Fig. 1. Schematic diagram of the proposed setup for two-channel image reconstruction.

whereas the field distribution that appears in the Fourier plane in the $-M$ diffraction order is

$$\int_{-\infty}^{\infty}\int_{-\infty}^{\infty} a(x', y')\exp[-i\phi(x', y')]\exp[-i(2\pi x x' + 2\pi y y')]\mathrm{d}x\mathrm{d}y = \left\{\int_{-\infty}^{\infty}\int_{-\infty}^{\infty} a(x', y')\exp[i\phi(x', y')]\exp[+i(2\pi x x' + 2\pi y y')]\mathrm{d}x\mathrm{d}y\right\}^* = H^*(-x, -y), \tag{4}$$

where the asterisks represent complex-conjugate functions. Therefore the reconstructions appearing in the $+M$ and the $-M$ diffraction orders at the Fourier plane are complex conjugated as well as 180° rotated with respect to each other.

3. Reconstruction of Different Intensity Patterns

Starting with the complex-amplitude functions displayed at the Fourier plane, $H(x, y)$ and $H^*(-x, -y)$, we now perform free-space propagation (FSP) from the Fourier plane to a distance Z_0 away from it (see Fig. 1). By virtue of the Fresnel approximation one obtains

$$f_1(x'', y'') = \mathrm{FSP}[H(x, y), Z_0] = \frac{\exp(ikZ_0)}{i\lambda Z_0}\exp\left[i\frac{k}{2Z_0}(x''^2 + y''^2)\right] \times \int_{-\infty}^{\infty}\int_{-\infty}^{\infty} H(x, y)\exp\left[i\frac{k}{2Z_0}(x^2 + y^2)\right] \times \exp\left[-i\frac{2\pi}{\lambda Z_0}(xx'' + yy'')\right]\mathrm{d}x\mathrm{d}y, \tag{5}$$

$$f_2(x'', y'') = \mathrm{FSP}[H^*(-x, -y), Z_0] = \frac{\exp(ikZ_0)}{i\lambda Z_0}\exp\left[i\frac{k}{2Z_0}(x''^2 + y''^2)\right] \times \int_{-\infty}^{\infty}\int_{-\infty}^{\infty} H^*(-x, -y)\exp\left[i\frac{k}{2Z_0}(x^2 + y^2)\right] \times \exp\left[-i\frac{2\pi}{\lambda Z_0}(xx'' + yy'')\right]\mathrm{d}x\mathrm{d}y. \tag{6}$$

Can the two distributions $f_1(x'', y'')$ and $f_2(x'', y'')$ represent two nonidentical intensity functions? We now release all restrictions on the displayed phase but demand that the amplitudes of those distributions match the desired output functions to be reconstructed.

To compute the necessary filter function, one first has to determine what function $H(x, y)$ can generate the desired distributions f_1 and f_2 [Eqs. (5) and (6)]. Such a function can be found by use of an iterative algorithm, if we bear in mind that the amplitude distributions of f_1 and f_2 are the constraints and their phase distributions are free parameters with no restrictions. The proposed iterative procedure is in the spirit of the well-known Lesem–Hirsch–Jordan (L–H–J) algorithm, also known as the Gerchberg–Saxton algorithm.[7] Adapting this algorithm to our needs requires that the two constraints in the reconstruction plane both be satisfied by the same function $H(x, y)$. The fact that $H(x, y)$ can contain amplitude as well as phase information provides adequate degrees of freedom that should be chosen properly by the iterative procedure. In Fig. 2 a flowchart of the iterative algorithm is presented.

Many criteria can be used to examine the quality of the reconstructed images and determine when the iteration process should be stopped. A popular criterion is the minimum absolute intensity error (MIE), defined as

$$\mathrm{MIE} = \sum_m \sum_n |(A_{m,n}{}^{\mathrm{desired}})^2 - (A_{m,n}{}^{\mathrm{obtained}})^2|, \quad (7)$$

whereas the intensity is normalized according to

$$\sum_m \sum_n (A_{mn}{}^{\mathrm{desired}})^2 = \sum \sum (A_{m,n}{}^{\mathrm{obtained}})^2 = 1. \quad (8)$$

One is free to choose the number of iterations or the convergence rate to determine when the process should be stopped. The result of those iterations is the function $H_1(x, y)$, defined in the Fourier plane. The filter itself will thus be the inverse Fourier transform of $H_1(x, y)$, which will be encoded, as indicated in Section 2.

4. Generalizations

A. Weighting Average

The algorithm described in Sections 2 and 3 allocated equal weight to the two complex amplitudes to be generated. However, one can think of applications in which one channel is more important than the other. The task of assigning greater importance to one channel can be achieved if the two contributions are weighted differently, so that

$$H_1{}^{\mathrm{new}}(x, y) = (w_1 H_1 + w_2 H_2), \quad (9)$$

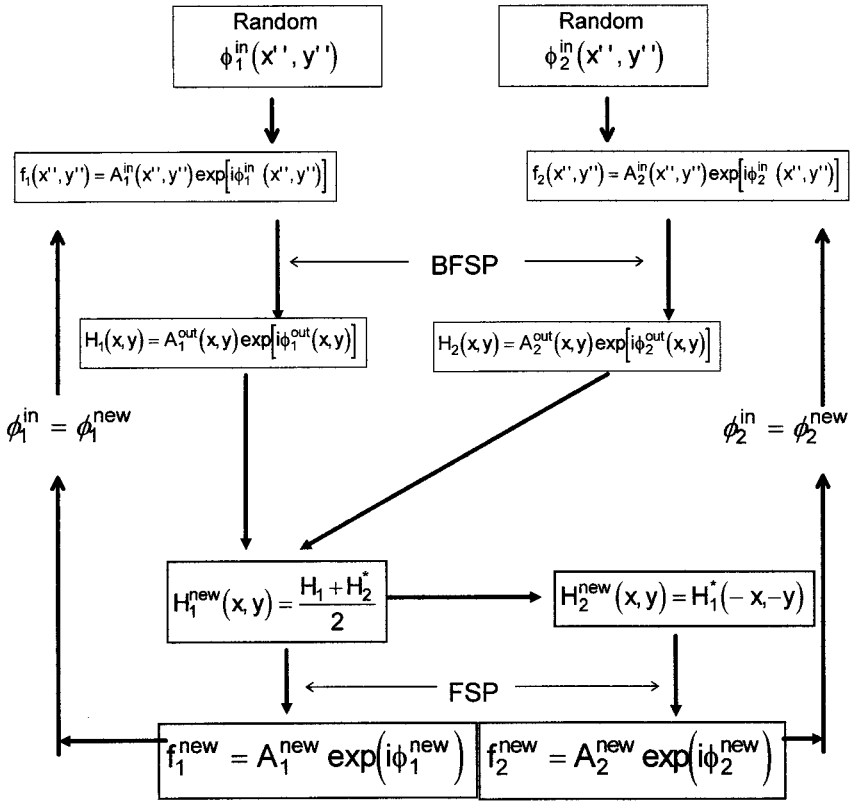

Fig. 2. Block diagram of the proposed algorithm for achieving different reconstructions along two symmetrical diffraction orders. BFSP, back-FSP.

where w_1 and w_2 are the weighting coefficients ($w_1 + w_2 = 1$) and H_1 and H_2 are defined in Fig. 3.

If unequal weighting coefficients are used, improved reconstruction is obtained for the high-priority channel, with reduced performance in the second, low-priority, channel. By proper selection of the weighting coefficients almost any desired MIE ratio can be obtained.

Several images and several weighting coefficients were tested. Good results can be obtained with a small number of iterations (fewer than 50). However, the suggested algorithm is rather complicated. Therefore other approaches have been considered.

B. Simplified Algorithm

It was indicated in Section 2 that, at the Fourier plane, one diffraction order is the complex conjugate and is a 180°-rotated version of its respective symmetrical order. However, starting with $H^*(-x, -y)$ and performing a back-FSP from $Z = 0$ to $Z = -Z_0$, one obtains

$$
\begin{aligned}
f_3(x'', y'') &= \mathrm{FSP}[H^*(-x, -y), -Z_0] \\
&= \frac{\exp(-ikZ_0)}{-i\lambda Z_0} \exp\left[-i \frac{k}{2Z_0}(x''^2 + y''^2)\right] \\
&\quad \times \int_{-\infty}^{\infty}\int_{-\infty}^{\infty} H^*(-x, -y)\exp\left[-i \frac{k}{2Z_0}(x^2 + y^2)\right] \\
&\quad \times \exp\left[+i \frac{2\pi}{\lambda Z_0}(xx'' + yy'')\right] dx\,dy \\
&= \left\{\frac{\exp(+ikZ_0)}{+i\lambda Z_0} \exp\left[+i \frac{k}{2Z_0}(x''^2 + y''^2)\right]\right. \\
&\quad \times \int_{-\infty}^{\infty}\int_{-\infty}^{\infty} H(-x, -y)\exp\left[+i \frac{k}{2Z_0}(x^2 + y^2)\right] \\
&\quad \left.\times \exp\left[-i \frac{2\pi}{\lambda Z_0}(xx'' + yy'')\right] dx\,dy\right\}^* \\
&= \left(\frac{\exp(ikZ_0)}{i\lambda Z_0} \exp\left[i \frac{k}{2Z_0}(x''^2 + y''^2)\right]\right. \\
&\quad \times \int_{-\infty}^{\infty}\int_{-\infty}^{\infty} H(x, y)\exp\left[+i \frac{k}{2Z_0}(x^2 + y^2)\right] \\
&\quad \left.\times \exp\left\{-\frac{2\pi}{\lambda Z_0}[x(-x'') + y(-y'')]\right\}\right)^* \\
&= f_1^*(-x'', -y''). \qquad (10)
\end{aligned}
$$

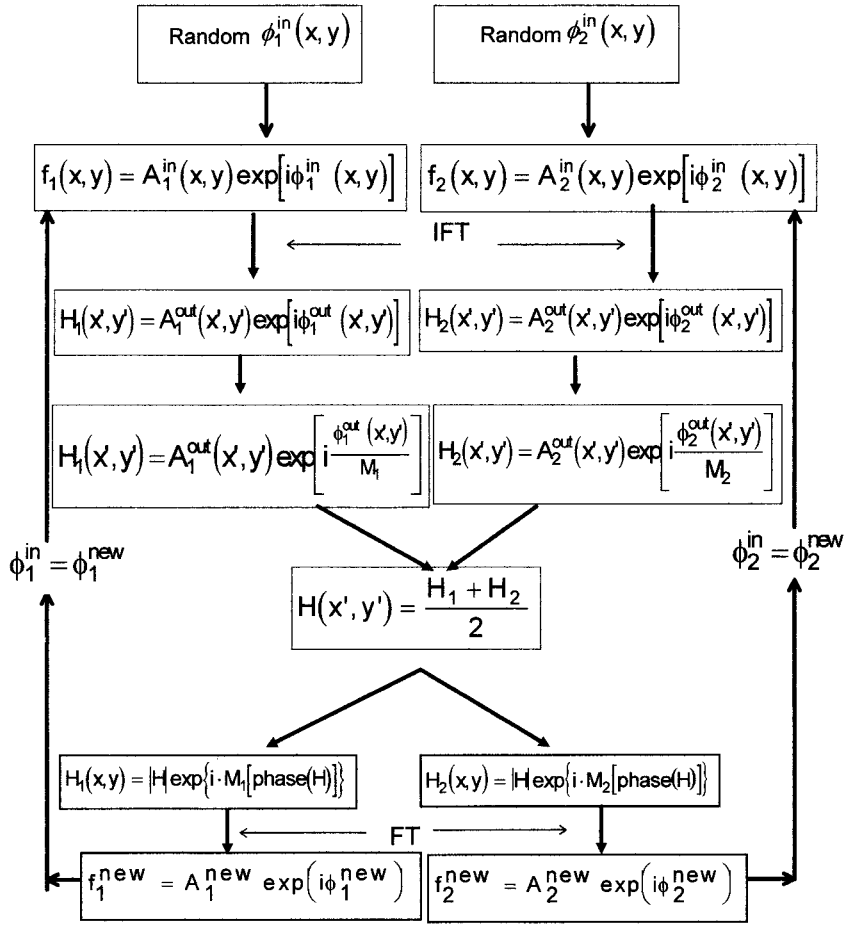

Fig. 3. Block diagram of the algorithm for reconstructing distributions along nonsymmetric diffraction orders. IFT, inverse Fourier transform.

We have thus found that the complex function generated after back-FSP to a distance $-Z$ in one channel is the complex conjugate and a 180°-rotated version of the function obtained after FSP to a distance $+Z$ in the corresponding symmetrical order beam. One can thus calculate the complex functions f_1 and f_2 at the $\pm Z$ planes for only one-diffraction-order distributions. This conclusion resembles the approach suggested in Ref. 6 whereby two different distributions were displayed in two locations along the Z axis. The difference is that, instead of arbitrarily choosing the planes of the reconstruction, we must choose the planes so as to fulfill the conjugate relation of equal separation from the Fourier plane. Thus two different channels are obtained at the $+Z$ plane (as well as at the $-Z$ plane) along two different diffraction orders or along a single order at the $\pm Z$ locations. After the two desired complex functions have been calculated, the complex function at the $Z = 0$ plane can be calculated, according to

$$H = w_1 H_1 + w_2 H_2, \tag{11}$$

where $H_1 = \mathrm{FSP}(f_1 + Z)$ and $H_2 = \mathrm{FSP}(f_2, -Z)$. The distribution H can be reconstructed by use of one of the detour phase encoding methods mentioned in Section 1 (see, for example, Refs. 1–4).

C. Arbitrary Diffraction Orders

So far only two symmetric diffraction orders have been analyzed. However, it is also possible to demand generation of two different intensities at any two diffraction orders along the Fresnel or the Fourier planes. We are no longer limited to the requirement that the orders should be along two different sides of the optical axis (this can be important because the zero order can be strong compared with the desired order and can obscure the desired patterns if left in the field of view). Moreover, wide-angle reconstruction can be obtained because the higher orders possess higher diffraction angles. The main drawback of using nonsymmetrical high orders is the relatively low diffraction efficiency of the higher orders. Indeed, the diffraction efficiency of the two reconstruction images will not be the same (except for the special case of symmetrical orders).

The approach is based on the fact that the phase information that propagates along different orders

Fig. 4. Two objects used for computer simulations and experimental tests.

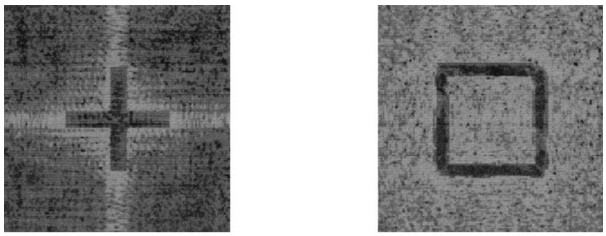

Fig. 5. Reconstruction achieved by use of the basic approach (the algorithm shown in Fig. 2) after 100 iterations ($w_1 = w_2 = 0.5$).

can be very different, as was indeed identified in Eq. (2). With Fourier plane reconstruction assumed and two desired orders (M_1 and M_2) chosen, the two reconstructed objects are given by

$$f_1(x'', y'') = \mathrm{FT}\{A(x', y')\exp[i\phi(x', y')M_1]\}, \tag{12}$$

$$f_2(x'', y'') = \mathrm{FT}\{A(x', y')\exp[i\phi(x', y')M_2]\}. \tag{13}$$

Therefore two patterns having different intensity distributions can be obtained. As discussed above, the two constraints can be achieved if phase freedom is allowed for the reconstructed images. A flowchart describing such an iterative process is shown in Fig. 3.

The process can be stopped by the same parameters that were discussed in Section 3. The

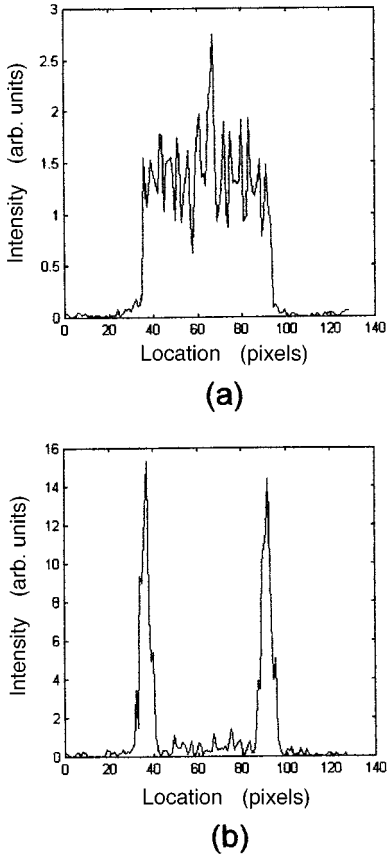

Fig. 6. Center-line horizontal intensity profile of Fig. 5.

weighting-coefficients approach can be used here, as well, to enhance the reconstruction of one pattern with respect to the other. Computer simulations as well as experimental results are provided in Sections 6 and 7.

A practical drawback of requiring reconstructions along diffracted beams corresponding to higher orders is that the phase accuracy [Eq. (2)] requires higher-resolution capabilities for filter fabrication. Indeed, to generate a specific phase shift in the Mth diffraction order according to the detour phase approach, one needs to locate the aperture in the filter with a resolution accuracy M times finer than that for the first order.

D. Four Separate Intensity-Pattern Reconstructions

So far only two separate intensity-pattern reconstructions have been discussed. However, one can use two orthogonal spatial coordinates to expand the currently proposed algorithm so that four images are reconstructed—two along the vertical axis and two along the horizontal one—following the approach described in Ref. 8. In that approach two different sets of diffracted beams are generated along the two axes, each of them able to be designed along the lines described in Section 3 (following the algorithm given in Fig. 2). After the two functions $H_{\text{horizontal}}$ and H_{vertical} are obtained in the Fourier plane, a Fourier transform operation is carried out, and the two new functions are encoded according to Ref. 8. The combination of the two approaches leads to four desired patterns of different intensity distributions, located along four different directions and two orthogonal axes. However, each channel suffers from a relatively low light efficiency because of the diffraction in the two dimensions.

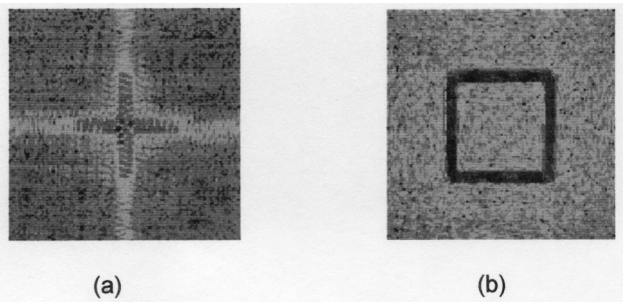

Fig. 8. Reconstruction achieved by use of the basic approach after 100 iterations with the weights $w_1 = 0.3$ and $w_2 = 0.7$.

5. Parameter Selection

Until now, the FSP distance Z was treated as a free parameter to be chosen. However, it is critical that it be chosen appropriately. Values that are too low do not allow the energy to be reshaped as desired, whereas values that are too high might cause aliasing in the computation process.

The minimal distance that makes it possible for the

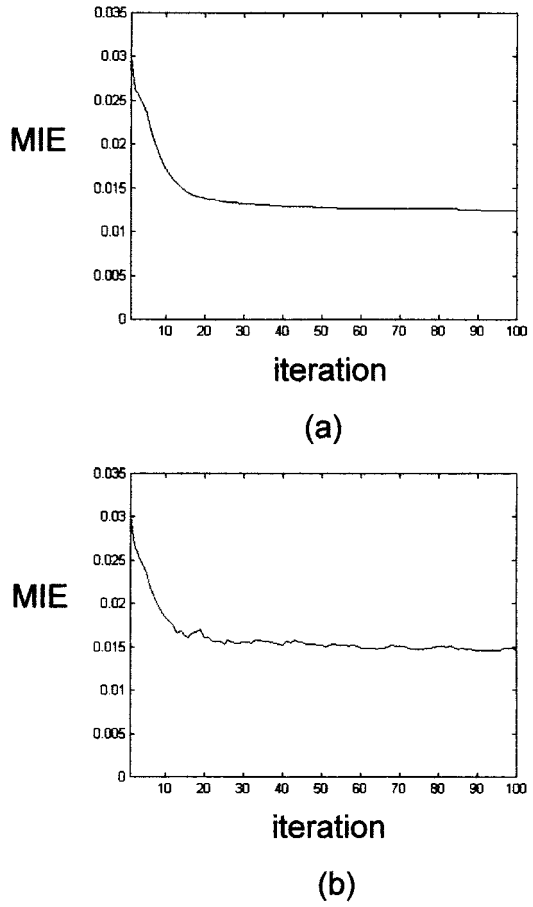

Fig. 7. MIE factor as a function of the number of iterations for the images reconstructed in (a) Fig. 5(a) and (b) Fig. 5(b).

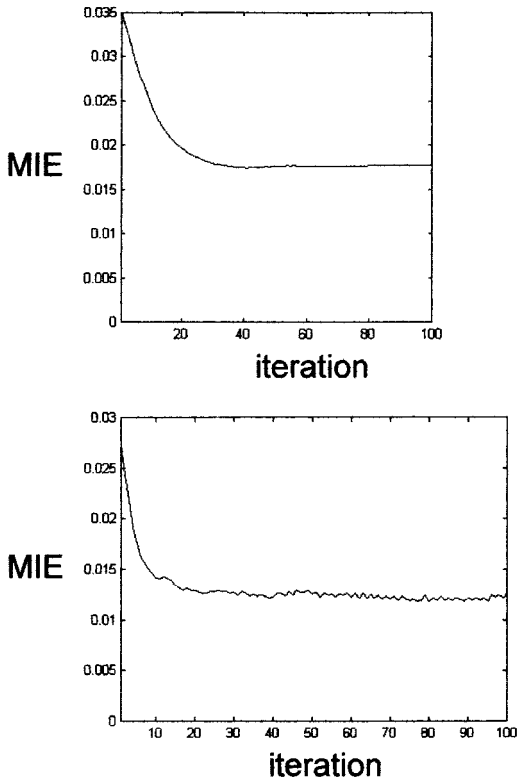

Fig. 9. MIE factor as a function of the iteration number for the images reconstructed in (a) Fig. 8(a) and (b) Fig. 8(b).

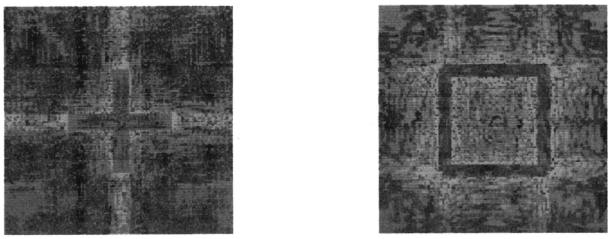

(a) (b)

Fig. 10. Reconstruction achieved by use of the simplified approach after 100 iterations ($w_1 = w_2 = 0.5$).

energy to be diffracted into any desired location at the output plane can be calculated by the angle of the diffraction caused by the Fourier plane structure, which is designed with sample intervals of δx. The first diffraction-order direction is given by

$$\theta = \lambda/\delta x, \tag{14}$$

in which small diffraction angles are involved (paraxial approximation); therefore $\sin(\theta) \approx \tan(\theta) \approx \theta$. If the actual object size is

$$L_X = N\delta x, \tag{15}$$

where N is the number of samples, the various diffraction orders will not overlap if

$$Z \geq L_x/\theta = (L_x)^2/\lambda N, \tag{16}$$

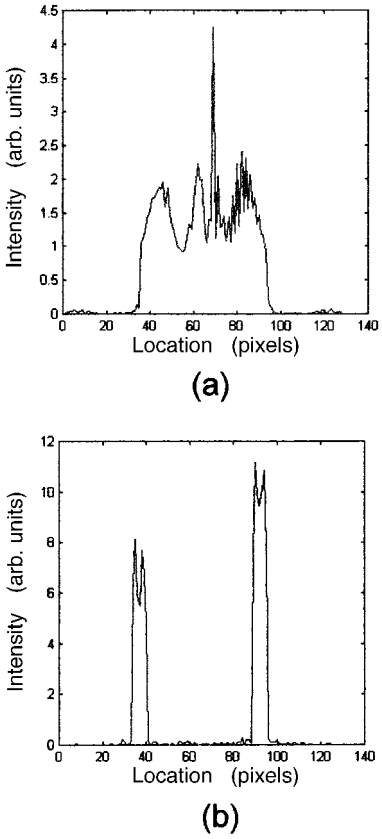

Fig. 11. Center-line horizontal intensity profiles of (a) Fig. 10(a) and (b) Fig. 10(b).

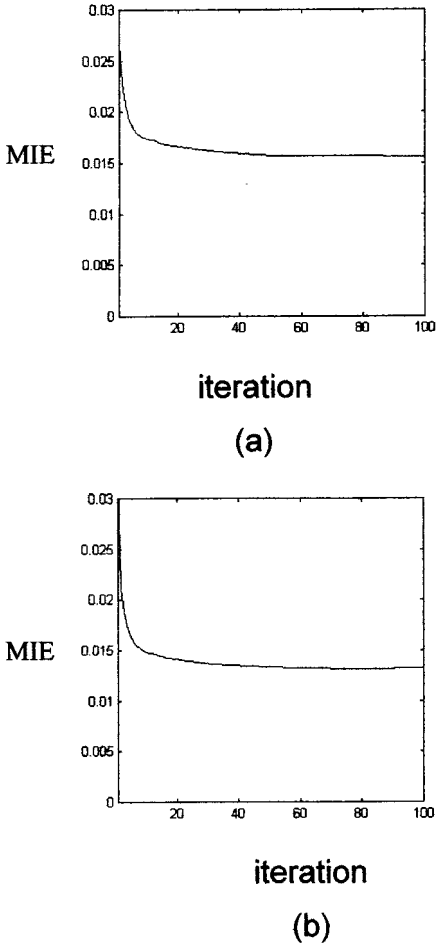

Fig. 12. MIE factor as a function of the number of iterations for (a) Fig. 10(a) and (b) Fig. 10(b).

under the same assumption of small diffraction angles.

Another consideration that has been observed for the computer calculations is the validity of using the fast Fourier transform subroutine for calculating the FSP. The fast Fourier transform assumes a periodic structure, and thus neighboring periods may enter into the sides of the frame (aliasing effect). Thus the

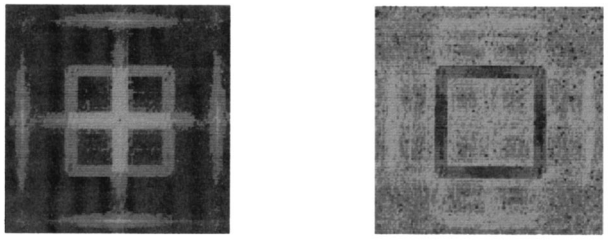

(a) (b)

Fig. 13. Reconstruction achieved by use of the nonsymmetric approach after 150 iterations ($w_1 = 0.25$ and $w_2 = 0.75$).

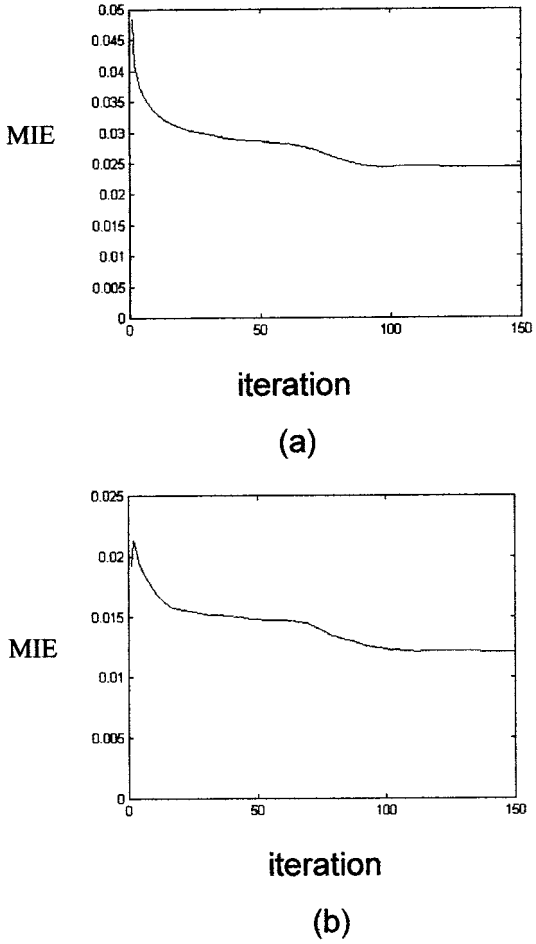

Fig. 14. MIE factor as a function of the number of iterations for (a) Fig. 13(a) and (b) Fig. 13(b).

maximum propagation distance is limited. An estimation of this value is given in Ref. 9:

$$Z \leq L_x/\theta = (L_x)^2/\lambda N. \tag{17}$$

The aliasing effect can be avoided if the size of the frame is increased, i.e., the two object planes are padded with zeros surrounding the objects themselves. Padding with a factor of F increases the permitted propagation distance by the same factor.

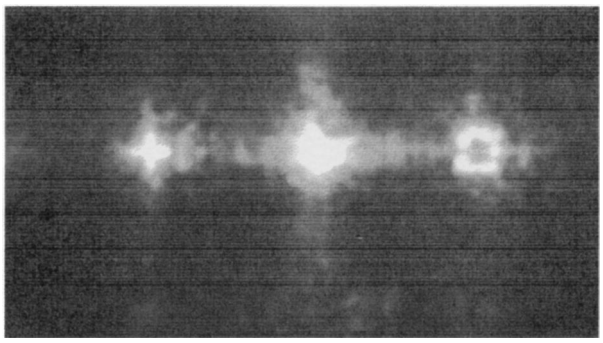

Fig. 15. Optical reconstruction of Fig. 4 achieved by use of the original approach ($w_1 = w_2 = 0.5$).

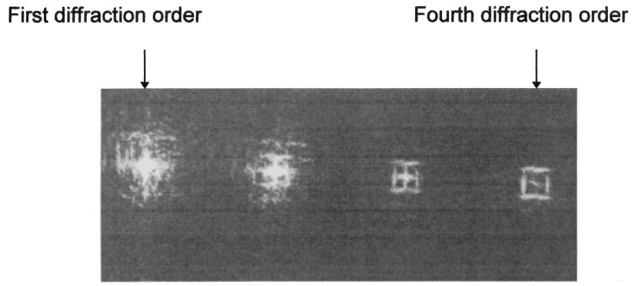

Fig. 16. Optical experimental reconstruction of Fig. 4 achieved by use of the nonsymmetric approach.

However, this solution might cause a problem in cases of limited spatial resolution.

6. Computer Simulations

Several computer simulations were carried out to demonstrate the capabilities of the proposed approach. The two objects to be reconstructed separately are shown in Fig. 4. The original patterns were defined by 64×64 pixels, but zero padding by a factor of 2 led to a 128×128 pixel size.

The reconstructions of these two objects achieved by means of the original approach with 50 iterations (as described in Fig. 3) are given in Fig. 5. The FSP distance is 1.2 m, and the wavelength is 0.63 μm. A 1 cm $\times$ 1 cm filter size was used. Equal weights were given to both functions. The center-line horizontal intensity profile is shown in Fig. 6. The MIE's of the objects as functions of the iteration number are given in Fig. 7.

The usefulness of the weighting-average approach is demonstrated in Fig. 8. For the same FSP distance and wavelength, weighting coefficients of 0.3 and 0.7 for the patterns shown in Figs. 5(a) and 5(b), respectively, were chosen. The MIE's for the images reconstructed in Fig. 8 are given in Fig. 9.

The two images (Fig. 4) were also reconstructed according to the simplified approach. The parameters were the same as for Fig. 5. In Figs. 10–12 the reconstruction image, a center-line horizontal intensity profile, and the MIE can be seen. Note that the MIE for the simplified approach is similar to that obtained when the basic approach was used.

Nonsymmetric order reconstructions were checked as well. The objects to be reconstructed are the cross and the square shown in Fig. 4. The reconstructions were designed to be obtained in the first and the fourth orders. The reconstructions and their MIE's are displayed in Figs. 13 and 14, respectively.

Fig. 17. New set of four objects used for the four-channel experiment.

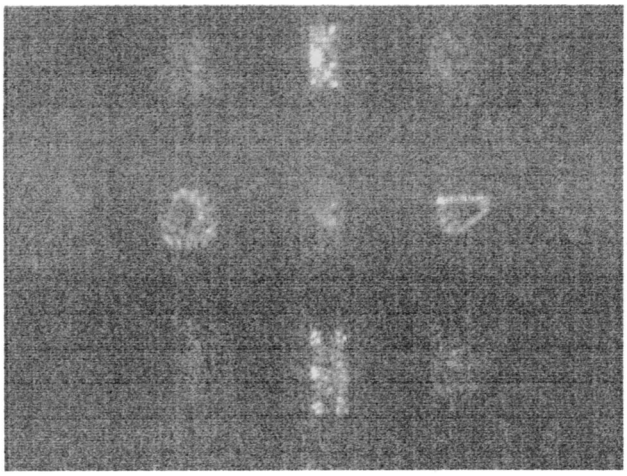

Fig. 18. Optical experimental reconstruction of Fig. 17 achieved by use of the four-channel approach.

7. Experimental Results

To test this process experimentally, we produced several filters. We encoded the filter function by changing the vertical dimensions of the aperture area, as described in Ref. 1. The computer-generated holograms were drawn on a Scitex plotter based on a laser-scanning device. The spot size of this machine is approximately 17 μm, with a resolution accuracy of 7 μm. The total hologram field was 13 mm $\times$ 13 mm and was divided into 128 $\times$ 128 cells of approximately 100 μm $\times$ 100 μm in size. More than 10 amplitude levels and even more phase levels were available.

The optical setup can be seen in Fig. 1. A He–Ne laser with a wavelength of 0.632 μm was used. The results were captured with the aid of a CCD camera. The optical reconstruction of the objects shown in Fig. 4 achieved by use of the original approach (Fig. 2) are shown in Fig. 15.

The general-order case was tested as well. The reconstruction of Fig. 4 can be seen in Fig. 16. The desired reconstruction is in the first and the fourth orders. A gradual change between the two objects can be noticed in the second and third orders.

To achieve four-channel reconstruction, we designed a new set of objects, as shown in Fig. 17. The encoding procedure was done according to the method reported in Ref. 8. The reconstruction is displayed in Fig. 18. Degraded quality was obtained because of a lack of spatial bandwidth.

8. Conclusions

A novel, to our knowledge, method that enables the generation of simultaneously different patterns along different diffraction orders has been suggested. Two different intensity patterns in two symmetrical diffraction orders can be displayed simultaneously by means of the basic approach presented. Reconstructions along symmetric diffraction orders can be obtained only in Fresnel planes and not in the Fourier plane. In addition, a general approach that makes it possible to obtain two different-intensity reconstructions along any two diffraction orders has also been suggested. Reconstructions along nonsymmetric orders of diffraction can be obtained in the Fourier domain as well. Four different intensity patterns can also be obtained by the application of the proposed method to the two orthogonal channels. Computer simulations and experimental results have showed that the reconstruction of various shapes with high efficiency and low noise was obtained. Therefore these methods can be used in various applications, such as optical communication, material processing, displays, and medical applications, in which only the intensity of the optical pattern is of significance.

References

1. G. R. Brown and A. W. Lohmann, "Complex spatial filtering with binary masks," Appl. Opt. **6,** 967–969 (1966).
2. A. W. Lohmann and D. P. Paris, "Binary Fraunhofer holograms, generated by computer," Appl. Opt. **6,** 1739–1749 (1967).
3. W. H. Lee, "Sampled Fourier transform holograms generated by computer," Appl. Opt. **9,** 639–643 (1970).
4. C. B. Burkhardt, "A simplification of Lee's method of generating holograms by computer," Appl. Opt. **9,** 1949 (1970).
5. F. Wyrowsky and O. Bryngdahl, "Iterative Fourier-transform algorithm applied to computer holography," J. Opt. Soc. Am. A **5,** 1058–1065 (1988).
6. R. G. Dorsch, A. W. Lohmann, and S. Sinzinger, "Fresnel ping-pong algorithm for two-plane computer-generated hologram display," Appl. Opt. **33,** 869–875 (1994).
7. R. W. Gerchberg and W. O. Saxton, "A practical algorithm for the determination of phase from image and diffraction plane figures," Optik (Stuttgart) **35,** 237–246 (1972).
8. D. Mendlovic and I. Kiryuschev, "Two channel computer generated hologram and its application for optical correlation," Opt. Commun. **116,** 322–325 (1995).
9. J. Garcia, D. Mas, and R. G. Dorsch, "Fractional Fourier transform calculation through the fast Fourier transform algorithm," Appl. Opt. **35,** 7013–7018 (1996).
10. J. W. Goodman, *Introduction to Fourier Optics*, 2nd ed. (McGraw-Hill, New York, 1996).